Chemistry–A European Journal
Research Article
doi.org/10.1002/chem.202400924
Chemistry Europe
European Chemical Societies Publishing
www.chemeurj.org

14-Membered Macrocyclic β-Diiminato Gold(II) – A New Member for the Gold(II) Complex Family?

Lukas Sorge,[a] Julian Link,[a] and Katja Heinze*[a]

The chemistry of molecular gold compounds is dominated by the oxidation states +I and +III. For the intermediate oxidation state +II with $5d^9$ electron configuration, dimerization or disproportionation of the gold(II) radicals is favored, so that only a few mononuclear gold(II) complexes have been isolated to date. The present study addresses the one-electron reduction of the macrocyclic gold(III) complex $[Au^{III}L]^+$ of the innocent β-diiminato ligand L^{2-} with a 14-membered macrocycle (L^{2-} = 5,7,12,14-tetramethyl-1,4,8,11-tetraazacyclotetradeca-5,7,12,14-tetraenato). Electrochemistry, spectroelectrochemistry and chemical reduction of $[Au^{III}L]^+$ monitored by UV/Vis, NMR and EPR spectroscopy together with density functional theory calculations reveal disproportionation of the initially generated but elusive gold(II) complex $Au^{II}L$ and provide guidelines for prospective stable mononuclear tetraaza-macrocyclic gold(II) complexes.

Introduction

The gold(II) ion, especially in molecular environments, typically disproportionates into Au^I and Au^{III} or dimerizes to $[Au^{II}–Au^{II}]$ with a gold(II)-gold(II) σ-bond, which can be bridged by a ligand or which can even be unsupported.[1–3] The origin of these typical reaction pathways lies in the strong relativistic expansion and thus destabilization of the 5d orbitals.[4–7] The half-filled $5d_{x2-y2}$ orbital is especially high in energy for the oxidation state +II in square-planar coordination geometry. Suitable environments to prevent disproportionation or dimerization are gas phase conditions in the mass spectrometer,[8] noble gas matrices[9–11] or zeolite encapsulation for a kinetic stabilization of mononuclear gold(II) species.[12] Transient gold(II) species have also been proposed as intermediates in homogenous catalysis,[2,13–19] artificial photosynthesis systems[20–22] or radical[23–26] and PCET[27,28] chemistry. In solid state materials, such as in simple salts $AuCl_2$ or $AuSO_4$, either a mixed-valence situation $Au^IAu^{III}Cl_4$ or dimerization $[Au^{II}(SO_4)]_2$ occurs.[1,29] A Au^{II}/Au^{III} mixed-valent perowskite $Cs_4Au^{II}Au^{III}{}_2Cl_{12}$ containing a square-planar coordinated gold(II) ion has been recently reported.[30] Alternatively, tailored ligand environments are essential for the kinetic and/or thermodynamic stabilization of mononuclear gold(II). Schröder and co-workers exploited the rigid nature of chelating 1,4,7-trithiacyclononane ligands to stabilize the gold(II) ion in $[Au^{II}([9]aneS_3)_2]^{2+}$ in a six-coordinate environment.[31] A first-order Jahn-Teller effect arising from the $5d^9$ electron configuration leads to an elongated octahedral complex geometry.[31] Even without the steric protection along the Jahn-Teller axis (z axis), mononuclear gold(II) can be stabilized as shown by the synthesis, isolation and full characterization of the tetraphenylporphyrinato gold(II) complex Au^{II}(tpp) as a truly mononuclear four-coordinate gold(II) complex (tpp^{2-} = 5,10,15,20-tetraphenylporphyrinato).[32]

The gold(II) ion in Au^{II}(tpp) is located in a [2+2] slightly distorted square-planar $[AuN_4]$ coordination environment with two shorter and two longer Au–N distances due to a second-order Jahn-Teller effect (Scheme 1).[32] Dimerization of Au^{II}(tpp)

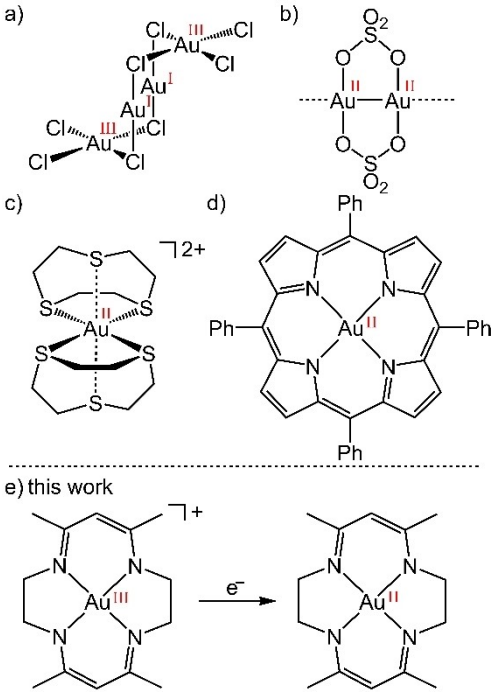

Scheme 1. Structural features of a) $AuCl_2$, b) $AuSO_4$, and molecular structures of c) $[Au^{II}([9]aneS_3)_2]^{2+}$ and d) Au^{II}(tpp) as well as e) the reduction of $[AuL]^+$ studied in this work.

[a] L. Sorge, J. Link, Prof. Dr. K. Heinze
Department of Chemistry,
Johannes Gutenberg University Mainz,
Duesbergweg 10–14, 55128 Mainz, Germany
E-mail: katja.heinze@uni-mainz.de

Supporting information for this article is available on the WWW under https://doi.org/10.1002/chem.202400924

with formation of a [Au^{II}–Au^{II}] σ bond from the half-filled 5d$_{x2-y2}$ orbitals is inhibited by the rigid porphine macrocycle blocking the xy plane. The formation of gold(I) as a result of disproportionation is energetically unfavorable due to the rigid coordination environment preventing the formation of linearly coordinated gold(I). Instead, the porphyrin ligand is reversibly reduced forming [Au^{II}(tpp$^{\bullet-}$)]$^-$. The latter radical anion is also thermodynamically comparably unfavorable so that the disproportionation constant of Au(tpp) amounts to merely $K_d = 3\times10^{-12}$ at room temperature.[32,33] As gold(I) is avoided, further potentially irreversible reduction or disproportionation reactions to gold(0) species are prevented as well.[32]

To question whether the porphine ligand is special in stabilizing gold(II) in a square-planar geometry by its rigid nature and its redox non-innocence prohibiting the formation of gold(I) and subsequent decomposition to gold(0), we investigated the redox chemistry of the known gold(III) complex [Au^{III}L]$^+$ with the redox-innocent dianionic macrocyclic 5,7,12,14-tetramethyl-1,4,8,11-tetraazacyclotetradeca-5,7,12,14-tetraenato ligand L^{2-} (Scheme 1). The parent gold(III) complexes [Au^{III}(tpp)]$^+$[34] and [Au^{III}L]$^+$[35,36] share a square-planar [AuN$_4$] coordination geometry with similar Au–N distances. However, the one-electron reduction of [Au^{III}L]$^+$ to Au^{II}L has not been reported yet. We describe the electrochemical, spectroelectrochemical and chemical reduction of [Au^{III}L]$^+$ and analyze the products by UV/Vis, EPR and NMR spectroscopy along with density functional theory (DFT) calculations to delineate ligand design strategies for four-coordinate molecular gold(II) complexes with respect to ring size, flexibility and redox activity of the macrocyclic ligand.

Results and Discussion

Synthesis and Spectroscopic Characterization. The gold(III) complex [AuL][PF$_6$] with the 14-membered macrocyclic ligand L^{2-} is prepared according to literature procedures[37,38] in a template reaction from [Au(en)$_2$]Cl$_3$ (en = ethylenediamine)[38] and acetylacetone followed by counter ion exchange with [NH$_4$][PF$_6$] in 60% overall yield. The air and moisture stable complex [AuL][PF$_6$] is characterized by multinuclear NMR (Figures S1–S4), ESI$^+$ mass spectrometry (Figure S7), IR spectroscopy (Figure S9) as well as UV/Vis absorption spectroscopy (Figures S20 and S21). The complex is sufficiently soluble in DMSO and DMF, but only poorly soluble in THF or 2-MeTHF. The ligand H$_2$L was prepared according to literature procedures[39] and characterized by ESI$^+$ mass spectrometry (Figure S8), ^{1}H and ^{13}C{^{1}H} NMR (Figures S5 and S6) and UV/Vis absorption spectroscopy for comparative reasons (Figures S23 and S24). Coordination of the gold(III) ion to the ligand is clearly indicated by the ESI$^+$ mass spectrometric data and the ^{1}H NMR coordination shift of the methylene and methine proton resonances from 3.31 and 4.44 ppm to 3.79 and 5.05 ppm, respectively. The PF$_6^-$ counter ion is detected by its ^{19}F and ^{31}P NMR resonances as well as its characteristic IR frequencies (Figures S3, S4 and S9).

The UV/Vis absorption spectrum of [AuL][PF$_6$] in DMSO is dominated by a band maximum at 286 nm ($\varepsilon = 4245$ M^{-1}cm^{-1}), an intense transition at 372 nm ($\varepsilon = 10730$ M^{-1}cm^{-1}) and a weaker shoulder located at ca. 450 nm ($\varepsilon = 652$ M^{-1}cm^{-1}) (Figure S20). These band maxima are rather weakly sensitive to the solvents DMSO vs. DMSO:DMF:2-MeTHF 1:5:5 (*v*/*v*) mixture (Figure S21). This specific solvent mixture combines sufficient solubility, redox stability of the reduced species for electrochemical experiments and formation of glass at low temperatures for EPR spectroscopic experiments. According to time-dependent DFT (TDDFT) calculations on [AuL]$^+$ the intense band arises from a π–π* transition within the β-diiminate units of the macrocyclic ligand, while the low-energy shoulder arises from a ligand-to-metal (LMCT; π_{ligand} to 5d$_{x2-y2}$) transition (Figure S20, Table S2). In agreement with this LMCT assignment, such a band is absent in the pro-ligand H$_2$L (Figures S23 and S24). The presence of an LMCT band suggests that gold(II) with 5d^9 electron configuration might be accessible by one-electron reduction.

Cyclic and Square Wave Voltammetry. The gold(III) complex [AuL][PF$_6$] shows a quasireversible reduction wave at −2.12 V and an irreversible wave at ca. −2.7 V vs. ferrocene/ferrocenium in DMSO:DMF:2-MeTHF 1:5:5 (*v*/*v*)/[^{n}Bu$_4$N][PF$_6$] (Figures 1 and 2). These values shift only slightly in DMSO/[^{n}Bu$_4$N][PF$_6$] (Figures S12 and S13).

The cathodic peak current $I_c(1)$ at −2.06 V exceeds that of its corresponding anodic counterpart $I_a(1)$ in the cyclic voltammogram (Figure 1b). The cathodic peak current $I_c(1)$ is also larger than the cathodic current at the second reduction wave $I_c(2)$ at −2.7 V (Figure 2). $I_c(1)$ is twice as large as that of the reductive FcH$^+$/FcH wave resulting from one equivalent of

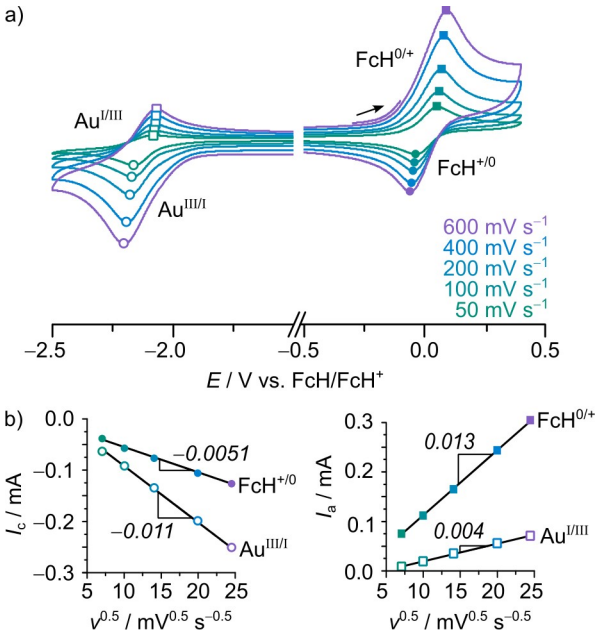

Figure 1. a) Cyclic voltammograms of [AuL][PF$_6$] and 1 equivalent ferrocene as internal standard 10^{-3} M in 0.1 M [^{n}Bu$_4$N][PF$_6$]/DMSO:DMF:2-MeTHF 1:5:5 (*v*/*v*) at different scan rates. Scan direction indicated by a black arrow. b) Cathodic and anodic peak currents I_c and I_a plotted against the square root of the corresponding scan rates. Slope of the linear fits given in italics.

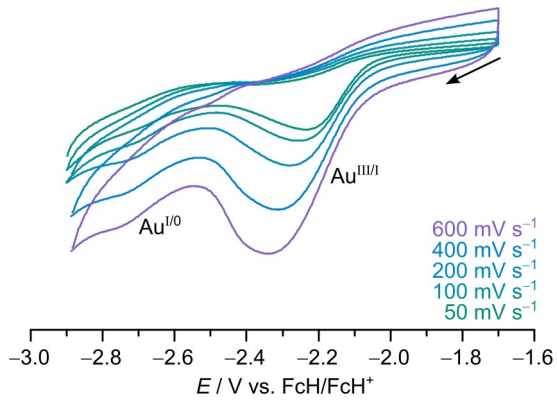

Figure 2. Cyclic voltammograms of [AuL][PF_6] 10^{-3} M in 0.1 M [^{n}Bu_4N][PF_6]/DMSO:DMF:2-MeTHF 1:5:5 (*v/v*) at different scan rates.

ferrocene as internal standard (Figure 1b). These data suggest, that $[Au^{III}L]^+$ is reduced in a quasi two-electron ($2e^-$) process to $[Au^{I}L]^-$ at around −2.06 V. The $[Au^{I}L]^-$ formed after the $2e^-$ reduction disproportionates into $Au^{II}L$ and $[Au^{0}L]^{2-}$. The latter species will irreversibly release the ligand with subsequent formation of gold(0). Hence, only one half of the current of the two-electron process is observed in the reverse anodic scan at −2.04 V (Figure 1). At higher potentials close to the FcH^+/FcH wave, the deposited gold(0) is re-oxidized, so that that the peak current of the FcH to FcH^+ oxidation increases correspondingly. At −2.7 V, residual, i.e. not yet disproportionated $[Au^{I}L]^-$ is reduced to gold(0).

Assuming a maximum peak difference of 0.1 V for the $[Au^{III}L]^+/Au^{II}L$ and $Au^{II}L/[Au^{I}L]^-$ processes, a disproportionation constant of $Au^{II}L$ of $K_d(Au^{II}L) \approx 0.02$ can be estimated. These estimated values can be compared to the respective potentials −0.97, −1.65 and −2.34 V of the reduction of $[Au^{III}(tpp)]^+$ to $Au^{II}(tpp)$ and to $[Au^{II}(tpp^{\bullet-})]^-$.[31] The disproportionation constant $K_d(Au^{II}(tpp)) = 3\times10^{-12}$ is thus smaller by orders of magnitude. Similarly, the disproportion constants for the anionic species $[Au^{I}L]^-$ and $[Au^{II}(tpp^{\bullet-})]^-$ of $K_d([Au^{I}L]^-) \approx 5\times10^{-8}$ and $K_d([Au^{II}(tpp^{\bullet-})]^-) = 2\times10^{-12}$ differ significantly. As the formal gold(0) complex $[Au^{0}L]^{2-}$ is unstable towards ligand loss, the quite large disproportionation constants of $Au^{II}L$ and $[Au^{I}L]^-$ provide an efficient and irreversible decay pathway towards gold(0).

A single $3e^-$ reduction of gold(III) to gold(0) has been observed for $[Au^{III}(cyclam)]^{3+}$, while $[Au^{III}(Me_4cyclam)]^{3+}$ shows three $1e^-$ reduction processes at 0.17, −0.09 and −0.90 V vs. SCE (cyclam = 1,4,8,11-tetraazacyclotetradecane).[40] These data together with the present data and that of $[Au^{III}(tpp)]^+$ demonstrate, that the macrocyclic ligand determines the susceptibility of gold(II) towards disproportionation.

Chemical Reduction. Potassium graphite KC_8,[41] potassium[42] or sodium anthracenide (Figures S17 and S18) are sufficiently reducing to address the first $2e^-$ reduction wave of $[Au^{III}L][PF_6]$. A solution of [AuL][PF_6] in DMSO:DMF:2-MeTHF 1:5:5 (*v/v*) was treated with one of these reductants and rapidly frozen by cooling with liquid nitrogen. Unfortunately, no EPR resonances (X-band) were observed, irrespective of the reductant employed. The EPR resonance of sodium anthracenide (Figure S18), however, is absent as well, suggesting a successful electron transfer. Obviously, disproportionation of the initially formed $Au^{II}L$ and $[Au^{I}L]^-$ is too fast for the duration of sample preparation and irreversible.

To detect the final products of the one-electron reduction, the gold(III) complex was reduced with one equivalent of KC_8 in DMSO:DMF: MeTHF 1:5:5 (*v/v*) over 2 h. After filtration, removal of the solvents and dissolution in CD_2Cl_2 a ^{1}H NMR spectrum was recorded (Figure 3). The ^{1}H NMR spectrum displays resonances, which can be assigned to $[Au^{III}L]^+$ (δ = 4.98, 3.82 and 2.22 ppm) and the pro-ligand H_2L (δ = 4.50, 3.38 and 1.87 ppm) in a 2:1 integral ratio. The NH proton resonance of H_2L is observed at δ = 11.60 ppm. The NH protons likely stem from the employed solvents. Consequently, one-electron reduction of $[Au^{III}L]^+$ is followed by several disproportionation reactions leading to gold(0), free ligand and back-formation of $[Au^{III}L]^+$ according to eq. 1.

$$3\ [Au^{III}L]^+ + 3\ e^- + 2\ H^+ \rightarrow Au^0 + H_2L + 2\ [Au^{III}L]^+ \quad (1)$$

Using one equivalent of sodium anthracenide as reductant (Figure S18) similarly leads to the formation of H_2L (Figure S19).

The 2:1 ratio of $[Au^{III}L]^+$ and H_2L after one-electron reduction of $[Au^{III}L]^+$ with KC_8 is also observed in the UV/Vis absorption spectrum of the filtered reaction mixture as shown by the sum spectrum of $[Au^{III}L]^+$ and H_2L in a 2:1 ratio (Figure 4).

Clearly, the disproportionation of the gold(II) and gold(I) species is fast enough to prevent their spectroscopic characterization. This is also consistent with the observation of isosbestic points during the spectroelectrochemical reduction showing the decrease of the $[Au^{III}L]^+$ absorption band (Figure S22). For the gold(II) complex $Au^{II}L$, TDDFT calculations predict a low-energy absorption band at 933 nm, which possesses metal-to-ligand charge transfer (MLCT) character, namely from the half-filled $5d_{x2-y2}$ orbital of Au^{II} to one β-diiminate unit of the ligand

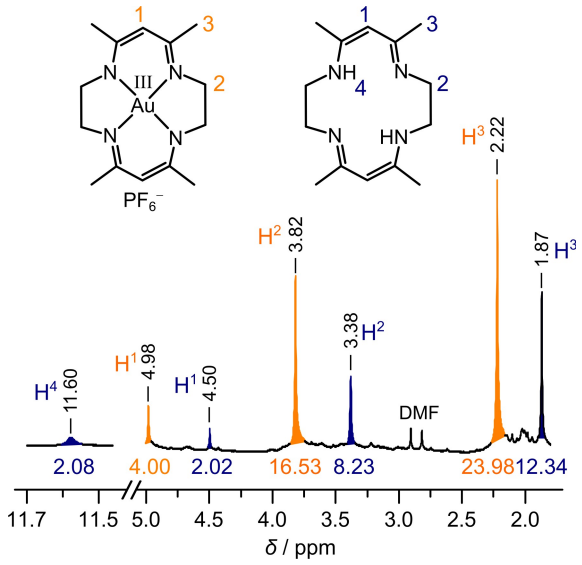

Figure 3. ^{1}H NMR spectrum of the reaction products of [AuL][PF_6] with 1 equivalent KC_8 in DMSO:DMF:2-MeTHF 1:5:5 (*v/v*). Spectrum recorded in CD_2Cl_2. Atom numbering given for proton assignments.

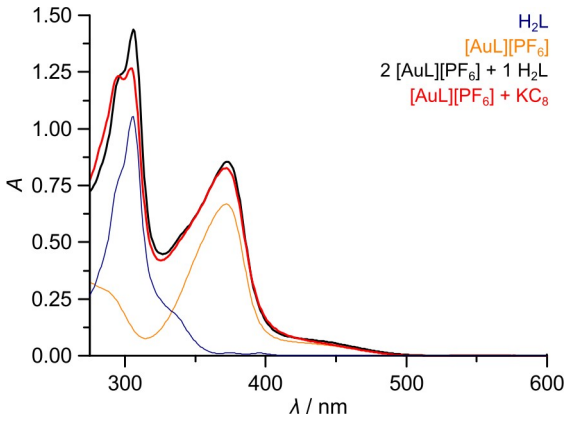

Figure 4. Absorption spectrum (red) of the reaction mixture after reduction of [AuL][PF_6] with 1 equivalent KC_8 in DMSO:DMF:2-MeTHF 1:5:5 (*v/v*). Absorption spectra of [AuL][PF_6] (orange), the pro-ligand H_2L (blue) and a sum spectrum of [AuL][PF_6] and H_2L in a 2:1 ratio (black).

(Figure S25, Table S3). However, no such absorption band could be detected during the spectroelectrochemical reduction (Figure S22). The TDDFT calculated transitions of the aurate(I) $[Au^{I}L]^-$ are uncharacteristic according to TDDFT calculations (Figure S26, Table S4) and thus $[Au^{I}L]^-$ might not be detectable in the reaction mixture at low concentrations.

Quantum Chemical Calculations. In order to delineate the differences between the reversible $[Au(tpp)]^{+/0/-}$ redox steps and the irreversible reductions of $[Au^{III}L]^+$ we optimized the geometries of $[AuL]^{+/0/-}$ as well as of $[Au(tpp)]^{+/0/-}$ complexes for comparison on the same level of theory including relativistic and solvent effects.

The gold(III) complex $[Au^{III}L]^+$ had been crystallized with various counter ions.[35,36,43,44] In all cases, a four-coordinate slightly twisted square-planar environment is found with essentially planar six-membered chelate rings and twisted five-membered chelate rings of the ethylene diamine parts of the macrocycle. The Au–N distances vary from 1.974 to 1.992 Å with Au–N = 1.974(2)–1.981(2) Å ([AuL][BPh_4]),[36] 1.988(4)–1.992(4) Å ([AuL][ReO_4]),[43] 1.981(3)–1.986(3) Å ([AuL][$AuBr_2$])[44] and Au–N 1.975(5)–1.9885(5) Å ([AuL][Br]).[35] In the DFT optimized geometry of $[AuL]^+$, the Au–N distances were calculated as 1.995–1.996 Å in reasonable agreement with the solid state structural data (Figure 5). The DFT calculated distances of $[Au(tpp)]^+$ of 2.029 Å agree with those of [Au(tpp)][ClO_4] (2.032(5)–2.033(5) Å) as well.[45] The shorter Au–N distances in $[Au^{III}L]^+$ as compared to $[Au^{III}(tpp)]^+$ likely arise from the smaller ring size of the macrocycle (14 vs. 16-membered rings) maintaining an essential square-planar [AuN_4] coordination. The stronger Au–N interactions in $[Au^{III}L]^+$ substantially raise the energy of the $5d_{x2-y2}$ orbital as compared to the energy of the $5d_{x2-y2}$ orbital in $[Au^{III}(tpp)]^+$ (Figure 6). This rather high energy of the $5d_{x2-y2}$ orbital accounts for the more cathodic reduction potential of $[Au^{III}L]^+$ (see above).

Reduction of $[Au^{III}L]^+$ and $[Au^{III}(tpp)]^+$ leads to the gold(II) complexes $Au^{II}L$ and $Au^{II}(tpp)$ with metal-centered spin densities of 0.374 and 0.328, respectively. In both cases, some spin density is delocalized onto the coordinating N atoms (0.116–

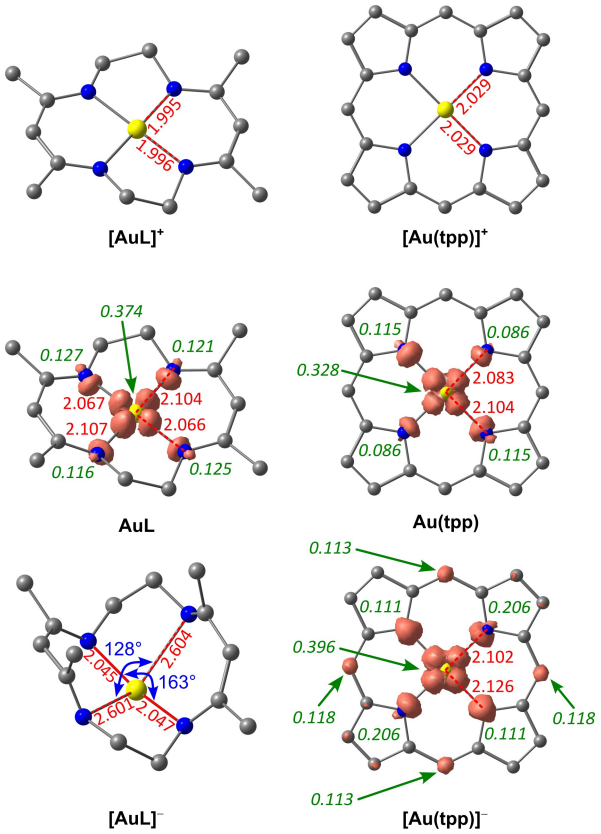

Figure 5. DFT optimized geometries of $[AuL]^+$, AuL, $[AuL]^-$ (left) and $[Au(tpp)]^+$, Au(tpp) and $[Au(tpp)]^-$ (right) with Au–N distances given in Å (red), angles given in deg (blue), Mulliken spin populations given in green (italics). Spin density plots at an isosurface value of 0.015 a.u. (orange). Hydrogen atoms and phenyl substituents omitted for clarity.

0.127 and 0.086–0.115, respectively). The metal-centered reduction of $[Au^{III}L]^+$ to $Au^{II}L$ increases the calculated Au–N bond lengths to 2.066/2.067/2.104/2.107 Å. Similarly, the calculated Au–N distances of $[Au^{III}(tpp)]^+$ increased to 2.083/2.104 Å in $Au^{II}(tpp)$ in agreement with the experimental data (2.0586(24)/2.0970(23) Å).[30] The differences between the *trans* Au–N bond lengths are significant and reproduced by the calculations in both cases with the bond length difference in $Au^{II}L$ (0.038 Å) being larger than that calculated for $Au^{II}(tpp)$ (0.021 Å). This symmetry-lowering had been suggested to arise from a second-order Jahn-Teller effect of the $(5d)^9$ electron configuration achieved by admixture of the $(5d)^8(6s)^1$ electron configuration.[32] Obviously, the L^{2-} macrocycle with ethylene bridges can better accommodate Au–N bond length changes than the more rigid tpp^{2-} macrocycle lacking aliphatic bridges. This higher flexibility becomes even more obvious in the aurates $[AuL]^-$ and $[Au(tpp)]^-$.

Due to the presence of a π^*(tpp) orbital of appropriate energy (Figure 6), the electronic structure of $[Au(tpp)]^-$ is considered as a ligand centered radical anion coordinated to gold(II) $[Au^{II}(tpp^{\bullet-})]^-$ with balanced Au–N distances of 2.102/2.126 Å instead of a gold(I) complex with a twofold coordination. On the other hand, L^{2-} lacks suitable ligand-centered π^* orbitals (Figure 6). Consequently, $[Au^{I}L]^-$ is a genuine gold(I)

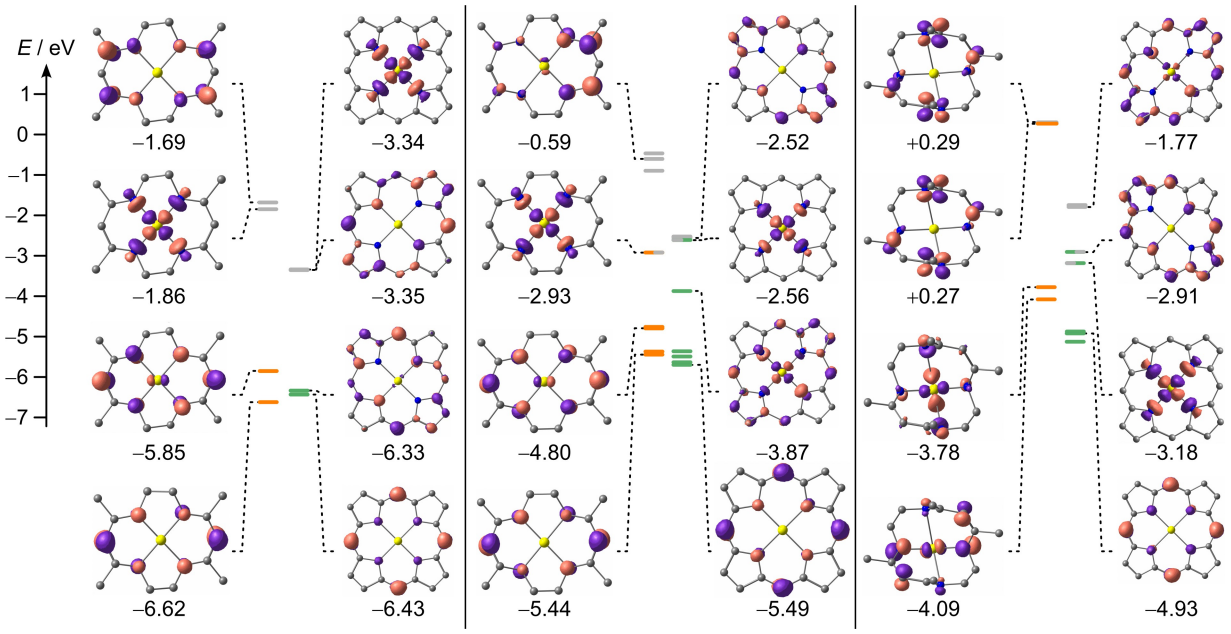

Figure 6. Molecular orbital diagrams for $[AuL]^+$/$[Au(tpp)]^+$ (left), AuL/Au(tpp) (center) and $[AuL]^-$/$[Au(tpp)]^-$ (right) and frontier molecular orbitals derived from DFT geometry optimized structures. Occupied molecular orbitals are indicated by filled, singly occupied α molecular orbitals by half-filled and unoccupied molecular orbitals by grey bars. Hydrogen atoms and phenyl substituents omitted for clarity. Isosurface values at 0.018 a.u.

species. As gold(I) prefers a linear coordination mode, the macrocyclic ligand distorts to accommodate gold(I) in a twofold coordination with Au–N distances of 2.045/2.047 Å and an N–Au–N angle of 163°. With this small angle the coordination geometry significantly deviates from linear. The other two Au–N distances increased to 2.601/2.603 Å with an N–Au–N angle of 128°. This leads to a strained out-of-plane coordination of the gold(I) ion and hence instability with respect to disproportionation and ligand dissociation.

Consequently, it is the instability of the gold(I) species $[Au^{I}L]^-$ that prevents the observation of the gold(II) complex $Au^{II}L$. If the gold(I) complex would be stable towards disproportionation followed by ligand loss it should be possible to observe gold(II) in the presence of gold(III) and gold(I) at its equilibrium concentration, even if its concentration might be low. The energies obtained from DFT calculations of $[AuL]^+$, AuL and $[AuL]^-$ yield a small positive $\Delta G = 8$ kJ mol^{-1} for the disproportionation and $K_d = 0.04$ at 298 K. Hence, even though $Au^{II}L$ might be weakly stabilized, the adjacent labile gold(I) oxidation state prevents its observation. In contrast, Au^{II}(tpp) and $[Au^{II}(tpp^{\bullet-})]^-$ are stable towards disproportionation, which closes the decay path to gold(0) and allows the isolation of Au^{II}(tpp).[32]

Conclusions

The gold(II) species $Au^{II}L$ with the flexible 14-membered macrocyclic ligand L^{2-} (L^{2-} = 5,7,12,14-tetramethyl-1,4,8,11-tetraazacyclotetradeca-5,7,12,14-tetraenato) is slightly stabilized towards disproportionation. This thermodynamic stability should allow its *in situ* characterization at its equilibrium concentration with $[AuL]^+$ and $[AuL]^-$ being present as well. However, the aurate(I) $[AuL]^-$ is susceptible towards irreversible disproportionation followed by ligand dissociation. This leads to an overall irreversible reduction to gold(0) so that the gold(II) and gold(I) complexes of L^{2-} are only transient species and remain elusive.

The moderate thermodynamic stability of $Au^{II}L$ as compared to Au^{II}(tpp) stems from its higher energy $5d_{x2-y2}$ orbital. The even more important insufficent kinetic inertness arises from the reactivity of the strongly distorted essentially two-coordinate aurate $[AuL]^-$ enabled by the flexible and redox-innocent L^{2-} macrocyclic ligand. The stability and hence the successful isolation of Au(tpp)[32] thus arises from the rigid and non-innocent 16-membered macrocycle that prevents the formation of distorted gold(I) species by formation of a ligand-centered radical with balanced Au–N distances instead.

Keys towards isolable mononuclear gold(II) complexes are thus employing i) rigid macrocyclic ligands that protect the gold(II) center from dimerization in the xy plane and ii) kinetically stable adjacent oxidation states. The present study shows that the macrocyclic ligand should stabilize the lower adjacent oxidation state, formally gold(I), for example by accommodating the additional electron in its π* system to prevent a disproportionation cascade to gold(0).

Supporting Information

The Supporting Information contains the employed methods, the synthesis procedures, spectroscopic, analytical and computational data (pdf) and the Cartesian coordinates of DFT optimized geometries (xyz). The authors have cited additional references within the Supporting Information.[46–61]

Acknowledgements

K. H. and L. S. thank the Deutsche Forschungsgemeinschaft DFG for funding via grant HE2778/16-1. Parts of this research were conducted using the supercomputer Elwetritsch and advisory services offered by the University of Kaiserslautern-Landau (https://hpc.rz.rptu.de). Open Access funding enabled and organized by Projekt DEAL.

Conflict of Interests

The authors declare no conflict of interest.

Data Availability Statement

The data that support the findings of this study are available in the supplementary material of this article.

Keywords: disproportionation · gold · macrocycle · redox chemistry

[1] D. B. Dell'Amico, F. Calderazzo, F. Marchetti, S. Merlino, *J. Chem. Soc. Dalton Trans.* **1982**, 2257–2260.
[2] a) K. Heinze, *Angew. Chem. Int. Ed.* **2017**, *56*, 16126–16134; b) J. C. Pérez-Sánchez, R. P. Herrera, M. Concepción Gimeno, *Dalton Trans.* **2024**, *53*, 382–393.
[3] a) H. Schmidbaur, *Acc. Chem. Res.* **1975**, *8*, 62–70; b) H. Schmidbaur, R. Franke, *Inorg. Chim. Acta* **1975**, *13*, 85–89; c) J. P. Fackler Jr., J. D. Basil, *Organometallics* **1982**, *1*, 871–873; d) V. W.-W. Yam, S. W.-K. Choi, K.-K. Cheung, *Chem. Commun.* **1996**, 1173–1174; e) S. K. Bhargava, F. Mohr, M. A. Bennett, L. L. Welling, A. C. Willis, *Organometallics* **2000**, *19*, 5628–5635; f) J. P. Fackler Jr., *Inorg. Chem.* **2002**, *41*, 6959–6972; g) K. Kitadai, M. Takahashi, M. Takeda, S. K. Bhargava, S. H. Privér, M. A. Bennett, *Dalton Trans.* **2006**, 2560–2571; h) J. Coetzee, W. F. Gabrielli, K. Coetzee, O. Schuster, S. D. Nogai, S. Cronje, H. G. Raubenheimer, *Angew. Chem. Int. Ed.* **2007**, *46*, 2497–2500; i) A. A. Mohamed, H. E. Abdou, J. P. Fackler Jr., *Coord. Chem. Rev.* **2010**, *254*, 1253–1259.
[4] L. F. Pašteka, E. Eliav, A. Borschevsky, U. Kaldor, P. Schwerdtfeger, *Phys. Rev. Lett.* **2017**, *118*, 023002.
[5] V. W.-W. Yam, E. C.-C. Cheng, *Chem. Soc. Rev.* **2008**, *37*, 1806–1813.
[6] H. Schmidbaur, *Gold Bull.* **2000**, *33*, 1–10.
[7] P. Pyykkö, *Angew. Chem. Int. Ed.* **2004**, *43*, 4412–4456.
[8] N. R. Walker, R. R. Wright, P. E. Barran, A. J. Stace, *Organometallics* **1999**, *18*, 3569–3571.
[9] T. Drews, S. Seidel, K. Seppelt, *Angew. Chem. Int. Ed.* **2002**, *41*, 454–456.
[10] S. Seidel, K. Seppelt, *Science* **2000**, *290*, 117–118.
[11] K. Seppelt, *Z. Anorg. Allg. Chem.* **2003**, *629*, 2427–2430.
[12] Z. Qu, L. Giurgiu, E. Roduner, *Chem. Commun.* **2006**, 2507–2509.
[13] B. Sahoo, M. N. Hopkinson, F. Glorius, *J. Am. Chem. Soc.* **2013**, *135*, 5505–5508.
[14] S. Kim, J. Rojas-Martin, F. D. Toste, *Chem. Sci.* **2016**, *7*, 85–88.
[15] X. Shu, M. Zhang, Y. He, H. Frei, F. D. Toste, *J. Am. Chem. Soc.* **2014**, *136*, 5844–5847.
[16] L. Huang, M. Rudolph, F. Rominger, A. S. K. Hashmi, *Angew. Chem. Int. Ed.* **2016**, *55*, 4808–4813.
[17] a) P. Veit, C. Volkert, C. Förster, V. Ksenofontov, S. Schlicher, M. Bauer, K. Heinze, *Chem. Commun.* **2019**, *55*, 4615–4618; b) M. P. Schrick, G. K. Ramollo, C.-M. S. Hirschbiegel, M. Fernandes, A. Lemmerer, C. Förster, D. I. Bezuidenhout, K. Heinze, *Organometallics* **2024**, *43*, 69–84.
[18] S. D. Waniek, C. Förster, K. Heinze, *Eur. J. Inorg. Chem.* **2022**, e202100905.
[19] S. Xia, W. Li, H. Chen, C. Zhu, J. Han, J. Xie, *J. Am. Chem. Soc.* **2023**, *145*, 26756–26764.
[20] S. Fukuzumi, K. Ohkubo, W. E. Z. Ou, J. Shao, K. M. Kadish, J. A. Hutchison, K. P. Ghiggino, J. J. Sintic, M. J. Crossley, *J. Am. Chem. Soc.* **2003**, *125*, 14984–14985.
[21] A. M. Brun, A. Harriman, V. Heitz, J. P. Sauvage, *J. Am. Chem. Soc.* **1991**, *113*, 8657–8663.
[22] E. Göransson, J. Boixel, J. Fortage, D. Jacquemin, H.-C. Becker, E. Blart, L. Hammarström, F. Odobel, *Inorg. Chem.* **2012**, *51*, 11500–11512.
[23] A. Johnson, R. J. Puddephatt, *J. Chem. Soc. Dalton Trans.* **1975**, 115–120.
[24] A. Johnson, R. J. Puddephatt, *J. Chem. Soc. Dalton Trans.* **1976**, 1360–1363.
[25] M. N. Hopkinson, A. Tlahuext-Aca, F. Glorius, *Acc. Chem. Res.* **2016**, *49*, 2261–2272.
[26] A. Tlahuext-Aca, M. N. Hopkinson, B. Sahoo, F. Glorius, *Chem. Sci.* **2016**, *7*, 89–93.
[27] S. Engbers, I. F. Leach, R. W. A. Havenith, J. E. M. N. Klein, *Chem. Eur. J.* **2022**, *28*, e202200599.
[28] K. M. Hess, I. F. Leach, L. Wijtenhorst, H. Lee, J. E. M. N. Klein, *Angew. Chem. Int. Ed.* **2024**, *63*, e202318916.
[29] M. S. Wickleder, *Z. Anorg. Allg. Chem.* **2001**, *627*, 2112–2114.
[30] K. P. Lindquist, A. Eghdami, C. R. Deschene, A. J. Heyer, J. Wen, A. G. Smith, E. I. Solomon, Y. S. Lee, J. B. Neaton, D. H. Ryan, H. I. Karunadasa, *Nat. Chem.* **2023**, *15*, 1780–1786.
[31] A. J. Blake, J. A. Greig, A. J. Holder, T. I. Hyde, A. Taylor, M. Schröder, *Angew. Chem. Int. Ed.* **1990**, *29*, 197–198.
[32] S. Preiß, C. Förster, S. Otto, M. Bauer, P. Müller, D. Hinderberger, H. Hashemi Haeri, L. Carella, K. Heinze, *Nat. Chem.* **2017**, *9*, 1249–1255.
[33] S. Preiß, J. Melomedov, A. Wünsche von Leupoldt, K. Heinze, *Chem. Sci.* **2016**, *7*, 596–610.
[34] E. B. Fleischer, A. Laszlo, *Inorg. Nucl. Chem. Lett.* **1969**, *5*, 373–376.
[35] V. A. Afanas'eva, I. V. Mironov, L. A. Glinskaya, R. F. Klevtsova, *Russ. J. Coord. Chem.* **2010**, *36*, 9–21.
[36] V. A. Afanas'eva, L. A. Glinskaya, D. A. Piryazev, S. A. Gromilov, P. E. Plyusnin, L. A. Sheludyakova, *Inorg. Chem. Commun.* **2017**, *83*, 70–75.
[37] B. P. Block, J. C. Bailar, *J. Am. Chem. Soc.* **1951**, *73*, 4722–4725.
[38] J.-H. Kim, G. W. Everett Jr., *Inorg. Chem.* **1979**, *18*, 3145–3149.
[39] T. Tokumitsu, T. Hayashi, *Bull. Chem. Soc. Jpn.* **1981**, *54*, 2348–2351.
[40] E. Kimura, Y. Kurogi, T. Koike, M. Shionoya, Y. Iitaka, *J. Coord. Chem.* **1993**, *28*, 33–49.
[41] S. A. Hodge, D. J. Buckley, H. C. Yau, N. T. Skipper, C. A. Howard, M. S. P. Shaffer, *Nanoscale* **2017**, *9*, 3150–3158.
[42] N. G. Connelly, W. E. Geiger, *Chem. Rev.* **1996**, *96*, 877–910.
[43] V. A. Afanas'eva, L. A. Glinskaya, D. A. Piryazev, S. A. Gromilov, *J. Struct. Chem.* **2015**, *56*, 787–791.
[44] V. A. Afanas'eva, L. A. Glinskaya, R. F. Klevtsova, I. V. Mironov, *Russ. J. Coord. Chem.* **2011**, *37*, 325–332.
[45] C.-M. Che, R. W.-Y. Sun, W.-Y. Yu, C.-B. Ko, N. Zhu, H. Sun, *Chem. Commun.* **2003**, 1718–1719.
[46] F. Neese, *WIREs Comput. Mol. Sci.* **2022**, *12*, 12753.
[47] A. D. Becke, *J. Chem. Phys.* **1993**, *98*, 5648–5652.
[48] B. Miehlich, A. Savin, H. Stoll, H. Preuss, *Chem. Phys. Lett.* **1989**, *157*, 200–206.
[49] F. Neese, F. Wennmohs, A. Hansen, U. Becker, *Chem. Phys.* **2009**, *356*, 98–109.
[50] D. A. Pantazis, X.-Y. Chen, C. R. Landis, F. Neese, *J. Chem. Theory Comput.* **2008**, *4*, 908–919.
[51] S. Miertuš, E. Scrocco, J. Tomasi, *Chem. Phys.* **1981**, *55*, 117–129.
[52] A. Schäfer, H. Horn, R. Ahlrichs, *J. Chem. Phys.* **1992**, *97*, 2571–2577.
[53] A. Schäfer, C. Huber, R. Ahlrichs, *J. Chem. Phys.* **1994**, *100*, 5829–5835.
[54] S. Grimme, J. Antony, S. Ehrlich, H. Krieg, *J. Chem. Phys.* **2010**, *132*, 154104.
[55] S. Grimme, S. Ehrlich, L. Goerigk, *J. Comput. Chem.* **2011**, *32*, 1456–1465.
[56] F. Weigend, R. Ahlrichs, *Phys. Chem. Chem. Phys.* **2005**, *7*, 3297–3305.
[57] D. A. Pantazis, X. Y. Chen, C. R. Landis, F. Neese, *J. Chem. Theory Comput.* **2008**, *4*, 908–919.
[58] F. Weigend, *Phys. Chem. Chem. Phys.* **2006**, *8*, 1057–1065.
[59] B. P. Block, J. C. Bailar, *J. Am. Chem. Soc.* **1951**, *73*, 4722–4725.
[60] J.-H. Kim, G. W. Everett Jr., *Inorg. Chem.* **1979**, *18*, 3145–3149.
[61] T. Tokumitsu, T. Hayashi, *Bull. Chem. Soc. Jpn.* **1981**, *54*, 2348–2351.

Manuscript received: March 5, 2024
Accepted manuscript online: April 16, 2024
Version of record online: May 17, 2024